

Concentration–Temperature Dependencies of Structural Relaxation Time in Trehalose–Water Solutions by Brillouin Inelastic UV Scattering[†]

S. Di Fonzo,[‡] C. Masciovecchio,[‡] F. Bencivenga,[‡] A. Gessini,[‡] D. Fioretto,[§] L. Comez,^{§,||}
A. Morresi,[⊥] M. E. Gallina,[⊥] O. De Giacomo,[#] and A. Cesàro^{*,#}

Sincrotrone Trieste, Strada Statale 14 km 163.5, Area Science Park, I-34012 Trieste, Italy, Dipartimento di Fisica, Università di Perugia, Via Pascoli, I-06100 Perugia, Italy, Dipartimento di Chimica, Università di Perugia, Via Elce di Sotto, 8, I-06100 Perugia, Italy, CRS SOFT INFM-CNR, c/o Dipartimento di Fisica, Università La Sapienza, P.le Aldo Moro 4, I-00185 Roma, Italy, Dipartimento di Biochimica, Biofisica e Chimica delle Macromolecole, Università di Trieste, Via L.Giorgieri 1, I-34127 Trieste, Italy

Received: July 28, 2007; In Final Form: October 10, 2007

A Brillouin scattering investigation has been carried out on trehalose–water solutions in a wide range of concentrations ($0 < \phi < 0.74$) in the ultraviolet regime. A complete set of data as a function of temperature ($-10\text{ °C} \leq T \leq 100\text{ °C}$) has been obtained for each concentration. The T – ϕ evolution of the system has been analyzed in terms of energy position and line width of inelastic peaks. These results have been used to derive the structural relaxation time, τ , of the system. This was found to be in the tens of picoseconds time scale, and its T dependence can be described with an activation (Arrhenius) law. Most importantly, a significant slowing down of the relaxation dynamics has been observed as trehalose concentration was increased. At low ϕ , the activation energy of the relaxation has been found to be consistent with literature data for pure water and comparable with intermolecular hydrogen bond (HB) energy. This evidence strongly supports the hypothesis that the main microscopic mechanism responsible for the relaxation process in trehalose solutions lies in the continuous rearrangement of the HB network. Finally, the results are discussed in terms of the evolution of the system upon increasing trehalose concentration, in order to provide a complete description of the viscoelastic stiffening in real biological conditions.

1. Introduction

Trehalose (α -D-glucopyranosyl- α -D-glucopyranoside) is known to be a nonreducing disaccharide made of two glucose units and, like most sugars, is a good vitrifying agent when its solutions are dried under appropriate conditions at biological temperatures. From a structural point of view, trehalose has the same chemical formula ($\text{C}_{12}\text{H}_{22}\text{O}_{11}$) and molecular mass ($M = 342.3$) as maltose and sucrose but a unique three-dimensional structure. The bioprotective properties of sugar trehalose have been known for almost two decades and are still a matter of extensive interest^{1–11} both from an academic point of view and for the potential applicative fall-out. In fact, it has been observed that several natural organisms, such as seeds, plants, fungi, bacteria, insects, hemolymph, and invertebrate animals (i.e., rotifers, nematodes, and tardigrades), produce trehalose at fairly high concentrations in the presence of harsh environmental conditions such as, for instance, drought, freezing, and ionizing radiations. Under a mechanism which is still controversial, they are capable of surviving for a long time in a state of suspended animation, so that their metabolic activity becomes quiescent or even undetectable (anhydrobiosis).

Four major hypotheses have been proposed to explain the stabilizing effect of trehalose on biostructures, but none of them are per se sufficient. The water-replacement hypothesis^{1–3} suggests that, upon drying, sugars can substitute water molecules by forming a water-like hydrogen bond (HB) network, thus, preserving the native structure of proteins in the absence of water. The vitrification hypothesis⁴ suggests that sugars found in anhydrobiotic systems protect biostructures through the formation of glasses, thereby reducing structural fluctuations and preventing protein denaturation or mechanical stresses. Furthermore, the higher glass transition temperature ($T_g = 121\text{ °C}$ in the pure anhydrous sugar) compared with similar disaccharides (e.g., sucrose: $T_g = 68.5\text{ °C}$) and other protectants (xylytol, sorbitol, glucose) could explain its greater efficiency. The destructuring-effect on the water HB hypothesis⁵ suggests that trehalose, compared with other disaccharides, facilitates a more extended hydration and binds water molecules more strongly, thus, preventing ice formation and the subsequent irreversible damage of biosystems. Finally the reversible-dehydration hypothesis^{6–8} refers to the formation of trehalose dihydrate nanocrystals and their subsequent reversible transformation into an anhydrous state during water removal, enhancing the biosystem stability.

In the past few years, a consensus has emerged in attributing trehalose's bioprotectant action to a synergic combination of the above factors, which cumulatively contribute to (i) a drastic slowing-down of molecular motions ensuring both structural conservation as well as chemical integrity and (ii) a preservation

[†] Part of the "Giacinto Scoles Festschrift".

* Author to whom correspondence should be addressed. E-mail: cesaro@units.it.

[‡] Sincrotrone Trieste.

[§] Dipartimento di Fisica, Università di Perugia.

^{||} CRS SOFT INFM-CNR Roma.

[⊥] Dipartimento di Chimica Università di Perugia.

[#] Dipartimento di Biochimica, Biofisica e Chimica delle Macromolecole, Università di Trieste.

of native conformations and morphologies of cellular biostructures during the dehydration–rehydration cycles.

Even though the exact mechanism responsible for bioprotective effectiveness is still unknown, it is clear that a complex array of interactions at structural, physiological, and molecular levels may play an important role. Therefore, a paramount, multidisciplinary investigation is still required in order to characterize structural and molecular interactions on binary trehalose–water solutions and on ternary trehalose–protein–water solutions. As far as interaction with water is concerned, and in accordance with the destructuring-effect hypothesis, molecular dynamic (MD) simulations found a larger hydration number for trehalose than for sucrose in the entire concentration range of 6–80 wt % and, moreover, the formation of long-range water structures has been observed⁹ up to the third solvation shell.¹⁰

Considerable experimental effort has been dedicated in recent years to the study of dynamical properties of trehalose solutions, both in bulk and in confined geometry.¹¹ These studies have involved depolarized light scattering, nuclear magnetic resonance, and Raman and neutron scattering.

With the aim of gaining a deeper understanding of the collective interactions which may occur in binary trehalose–water solutions, in the present work, propagating collective excitations have been determined by Brillouin inelastic ultraviolet scattering (IUVS) at $\lambda = 244$ nm incident photon wavelength. Measurements have been carried out in a wide range of trehalose concentrations ($0 < \phi < 74$ wt %) and temperatures (-10 °C $< T < +100$ °C). The T – ϕ evolution of the system has been analyzed in terms of energy positions and linewidths of inelastic excitations in the dynamic structure factor, $S(Q, \omega)$. These results have been further correlated with the structural relaxation time, τ , of the system, and its evolution with increasing concentration and decreasing temperature is discussed in details.

In general, density wave propagation in fluids perturbs their local structure. New equilibrium configurations are then locally restored by means of energy transfer from sound waves toward some internal degrees of freedom. These dynamical processes are usually called relaxation processes. Different relaxation processes can take place, according to the specific degree of freedom involved in the energy redistribution. Among them, structural relaxation is of major interest in the physics of glass formers, since it involves the cooperative readjustments of local structures responsible, for example, for glass formation. These processes are characterized by a time scale, τ , with a sharp temperature dependence roughly paralleling that of viscosity.¹² If the relaxation time scale is much shorter than the period of the acoustic wave, T_w , the internal fluid rearrangements are so fast that the system can reach its local equilibrium configuration within the period of density wave propagation, which therefore propagates adiabatically, that is, over successive local equilibrium states. This is the so-called hydrodynamic or viscous regime that characterizes the low-frequency acoustic propagation in simple fluids. If density waves with $T_w \ll \tau$ are probed, internal fluid rearrangements are indeed too slow, and consequently, the system cannot equilibrate within a propagation period. In this case, the energy carried by the density wave cannot be efficiently dissipated, and therefore, it propagates elastically, that is, with substantially reduced energy losses. This limiting behavior is commonly referred to as the elastic regime. In the intermediate, viscoelastic, regime, T_w is comparable with τ , and therefore, relaxation and density wave propagation mechanisms are strongly coupled.¹³ The occurrence of a

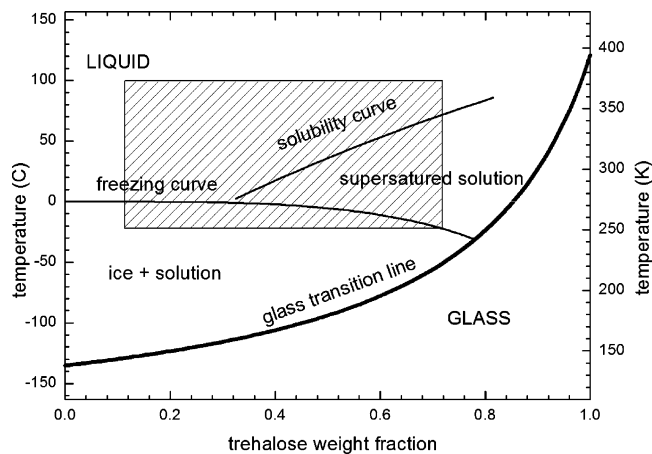


Figure 1. Phase diagram of water–trehalose solutions. The freezing and solubility curves were taken from refs 16 and 17. The glass transition line was calculated according to Gordon–Taylor equation,¹⁸ using the data reported by Chen et al.¹⁹ The shaded region indicates the ϕ – T ranges investigated in the present work (see Table 1).

TABLE 1: Measured Samples: Weight Fraction, ϕ , Number of Water Molecules Per Trehalose, n^* , Explored Temperature Ranges, Glass Transition Temperature, T_g , Average Density, $\bar{\rho}$, and Momentum Transfer Values, \bar{Q} , Are Reported

ϕ	n^*	T_{\min} (°C)	T_{\max} (°C)	T_g (°C)	$\bar{\rho}$ (Kg/m ³)	\bar{Q} (nm ⁻¹)
0	∞	1.5	30	-135	997.79	0.0712
0.15	107	0.0	89.7	-126.4	1046.50	0.0722
0.32	41	-4.2	89.8	-114.7	1125.02	0.0738
0.38	31	15.4	95.07	-108.6	1148.93	0.0744
0.42	26	-2.5	95.1	-103.4	1176.72	0.0750
0.47	21	-11.15	69.85	-96.9	1213.98	0.0757
0.59	13	-3.15	86.85	-79.6	1268.25	0.0769
0.74	7	-12.75	94.85	-45.6	1357.42	0.0788

relaxation phenomenon can be experimentally observed either by varying the period of the probed density (sound) wave or by varying the relaxation time itself. The former task can be accomplished, for example, by changing the momentum transfer, $Q \propto 1/T_w$, while the latter goal is usually achieved by varying the sample temperature. This paper will show that trehalose–water solutions in real biological conditions can be studied, at best, with IUVS since, thanks to the unique Q range probed by this technique, $T_w \approx \tau$, and therefore, sensitivity to the structural relaxation processes is maximized.

Although a very preliminary experiment of this kind in highly concentrated ($\phi \approx 80$) trehalose–water solutions was previously reported by some of us,¹⁴ the present detailed study of viscoelastic response in biological conditions as a function of both T and ϕ outlines some features of the uniqueness of the present IUVS experiments in adding important new knowledge about these complex biophysical systems.

2. Experimental Description

a. Sample Preparation. Trehalose dihydrate with purity greater than 99% was purchased from Sigma. Particular attention was paid in order to select a high purity sample with reduced metal content so as to avoid fluorescence caused by UV-induced electronic excitations in metals. After several tests, the product Sigma-T9449, extracted from corn starch,¹⁵ was identified as the best candidate and only in one case was another product used, resulting in low quality spectra.

The solutions were prepared by weight, dissolving the sugar in double distilled and deionized water and by stirring and

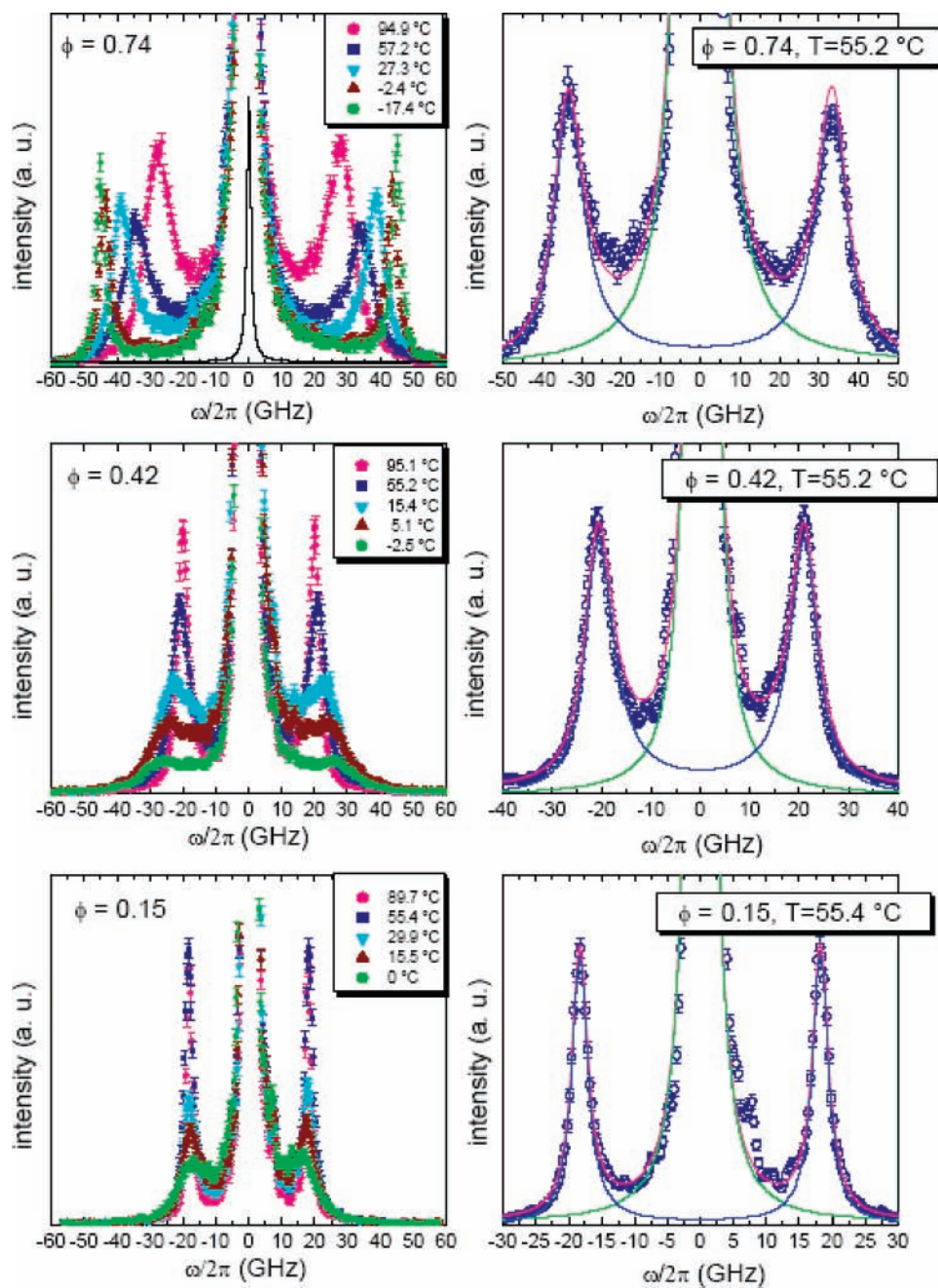


Figure 2. Left panels: set of representative IUVS spectra at three different weight concentrations: $\phi = 0.74$, $\phi = 0.42$, and $\phi = 0.15$. The solid line shown together with the spectra at $\phi = 0.74$ (black curve) is the overall instrumental resolution function. Right panels: three examples of experimental spectra, corresponding to $T = 55.2$ or 55.4 °C, are compared with the respective best fit results (red solid line). The elastic (green line) and inelastic (blue line) contributions are indicated as well. The spectra are normalized to the elastic peak intensity.

heating until the corresponding dihydrate solubility point was reached. Table 1 summarizes the different ϕ values probed in our experiments and the corresponding number of water molecules per trehalose, n^* . The explored conditions include ϕ – T values outside the thermodynamic stability limits of the homogeneous liquid phase. In general, crystallization is hampered by low temperatures (below 0 °C) and high concentrations, because of the high viscosity and weak nucleation processes. Nonetheless, occasional whitish opalescence was observed, precluding the feasibility of the experiment. Therefore, only metastable clear solutions have been effectively investigated as, only in that case, the scattering intensity could be properly measured.

Figure 1 reports the phase diagram of water–trehalose solutions. The shaded region indicates the investigated ϕ – T

ranges (see also data of Table 1). The solubility curve of dihydrate trehalose freezing and glass transition lines are indicated as well.

b. IUVS Measurements. IUVS measurements were carried out at the beamline 10.2 of the Elettra synchrotron radiation laboratory in Trieste.²⁰ The UV source was a frequency-doubled, CW output argon ion laser delivering a single-mode beam at $\lambda = 244$ nm (typical power ≈ 5 mW). The solutions were contained in a 2 mL cell placed in the beamline experimental chamber. This cell had two optically polished sapphire windows (3 mm thickness, 20 mm diameter) sealed by Teflon O-rings. The beam optical path-length in the cell was 10 mm. The sample spot size in the focal plane was $300 \times 200 \mu\text{m}^2$ (fwhm). The signal, scattered in the nearly backward direction ($\theta = 172^\circ$), was energy-analyzed by a normal incidence Czerny–Turner

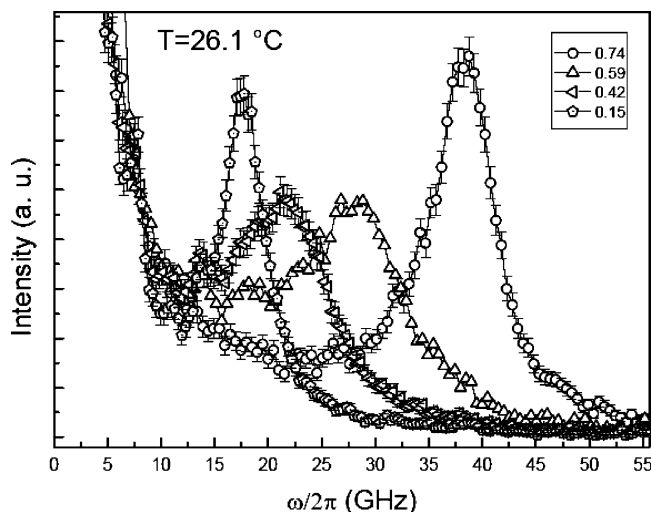


Figure 3. Representative IUVS spectra (raw data normalized for the elastic peak intensity) at four different weight concentrations $\phi = 0.74$, 0.59 , 0.42 , and 0.15 at the same indicated biological temperature: $T = 26.1$ °C.

analyzer²¹ and finally detected by a Peltier cooled CCD detector with $13.5 \times 13.5 \mu\text{m}^2$ pixel size and 20% quantum efficiency. The momentum transfer was calculated using the equation: $Q = (4\pi/\lambda)n \sin(\theta/2)$, where n is the refractive index, which was directly measured with an accuracy of the order of $5e^{-4}$ using a new method based on a modification of the fixed angle of incidence method for a hollow prism.²² The overall experimental energy and momentum resolutions were typically around 1.4 GHz ($\Delta E/E \approx 10^{-6}$) and 0.004 nm^{-1} ($\Delta Q/Q \approx 0.05$), respectively. Spectra were collected by varying the sample temperature in the ranges indicated in Table 1. A liquid nitrogen cryostat and a sample heater were used to scan the temperature, which was controlled with a K-type thermocouple. Temperature stability was greater than 0.1 °C during each spectrum acquisition (≈ 30 min). A moderate vacuum (10^{-6} mbar) was applied in the sample chamber during cooling in order to avoid air condensation.

3. Results and Discussion

a. ϕ - T Dependencies of Raw Data. Figure 2 (left panels) reports a set of representative IUVS spectra of samples corresponding to $\phi = 0.74$, $\phi = 0.42$, and $\phi = 0.15$. The occurrence of a relaxation process that matches the reciprocal frequency of the longitudinal modes can be directly noticed by looking at the raw data. In particular, a clear shift of inelastic peak positions toward higher energies is observed for $\phi = 0.42$ and 0.74 as the temperature decreases, while almost constant positions are observed at $\phi = 0.15$. Moreover, the energy positions of inelastic peaks at constant temperature notably increase with trehalose concentration.

To reinforce the construction of this concept, Figure 3 reports IUVS spectra at four different weight concentrations $\phi = 0.74$, 0.59 , 0.42 , and 0.15 and at the biological temperature of $T = 26.1$ °C. At this temperature, the addition of trehalose shifts the maximum of the inelastic peak toward higher energies and shrinks its width, thus, indicating that the internal degrees of freedom become too slow to efficiently dissipate the energy of the acoustic wave, as is expected for a solid-like, that is, frozen, medium.

A scrutiny of the T -dependence of inelastic peak widths shows, as the temperature decreases, a sharpening for $\phi = 0.74$ and a broadening for $\phi = 0.42$ and $\phi = 0.15$. In the frame of

the viscoelastic theory, the former case can be interpreted as a transition, undergone by inelastic excitations, from the maximum of the structural relaxation to the elastic limit. On the other hand, the latter two cases can be interpreted as the transition of the longitudinal mode away from the viscous (adiabatic) limit to the maximum of the structural relaxation.

b. Spectral Analysis and Fitting Procedure. According to the standard theory of Brillouin scattering in liquids and glasses,²³ the scattered intensity is directly proportional to the dynamic structure factor, $S(Q, \omega)$. In order to extract quantitative information on the T - ϕ dependencies of the line shape parameters, $S(Q, \omega)$ has been modeled by the sum of a δ function and a DHO function,²⁴ accounting for elastic and inelastic contributions, respectively:

$$S(Q, \omega) = A\delta(\omega) + B \frac{\omega_b^2(Q)\Gamma_b(Q)}{(\omega^2 - \omega_b^2(Q))^2 + \omega^2\Gamma_b^2(Q)} \quad (1)$$

where ω_b and Γ_b correspond to the position and line width (fwhm) of inelastic excitations. The intensity A of the central spectral line is mostly due to spurious scattering from the sample environment. The model reported in eq 1 has been properly convoluted with the instrumental resolution function and scaled by an arbitrary intensity factor. A flat background contribution, mostly due to the electronic noise of the detection system, was previously subtracted from the raw data. The fit procedure consists of a χ^2 minimization based on a standard nonlinear least-squares Levenberg–Marquardt algorithm.²⁵ The quality of our results can be appreciated in Figure 2 (right panels), where the measured spectra (open blue circles) are compared with the best fit line shape (red solid line). The T dependencies of ω_b and Γ_b are reported in Figure 5 for some selected ϕ values. Both of these hypersonic parameters show clear temperature dispersion, highlighting the presence of an active relaxation process in the experimental window. Moreover, such a dispersion shifts toward higher temperatures with increasing ϕ . In order to emphasize the effects of the relaxation, the attenuation per wavelength spectrum, $\alpha\lambda = \pi \Gamma_b(Q)/\omega_b(Q)$, is reported in Figure 4 (inset of right panel) for some representative ϕ values.

In the spectral region around Brillouin lines, the parameters ω_b and Γ_b are related to the real (M') and imaginary (M'') parts of the longitudinal elastic modulus, respectively:²⁶

$$M'(\omega_b) = \rho(\omega_b^2/Q^2) \quad \text{and} \quad M''(\omega_b) = \rho\omega_b(\Gamma_b/Q^2) \quad (2)$$

Both of these parameters are sensitive to the presence of an active relaxation whose time scale is of the order of ω_b^{-1} . In particular, within the hypothesis that the leading relaxation contribution in this frequency window can be modeled either by a Debye^{13,27–29,30–32} or a Cole–Davidson^{33,34} relaxation function, the quantity M'' , in the low-frequency regime ($\omega_b\tau \ll 1$), can be expressed as follows:^{26,27}

$$M''(\omega_b) = \rho\omega_b\Delta\tau/Q^2 \quad (3)$$

where Δ is the structural relaxation strength.^{29,30–32} Therefore, by simple substitution, one can write:

$$\Gamma_b = \Delta\tau \quad (4)$$

Usually, in the presence of a thermally activated relaxation process, the temperature dependence of the relaxation time can be written as: $\tau(T) = \tau_0 \exp(E_a/k_B T)$, where E_a and k_B are the activation energy of the relaxation and the Boltzmann constant,

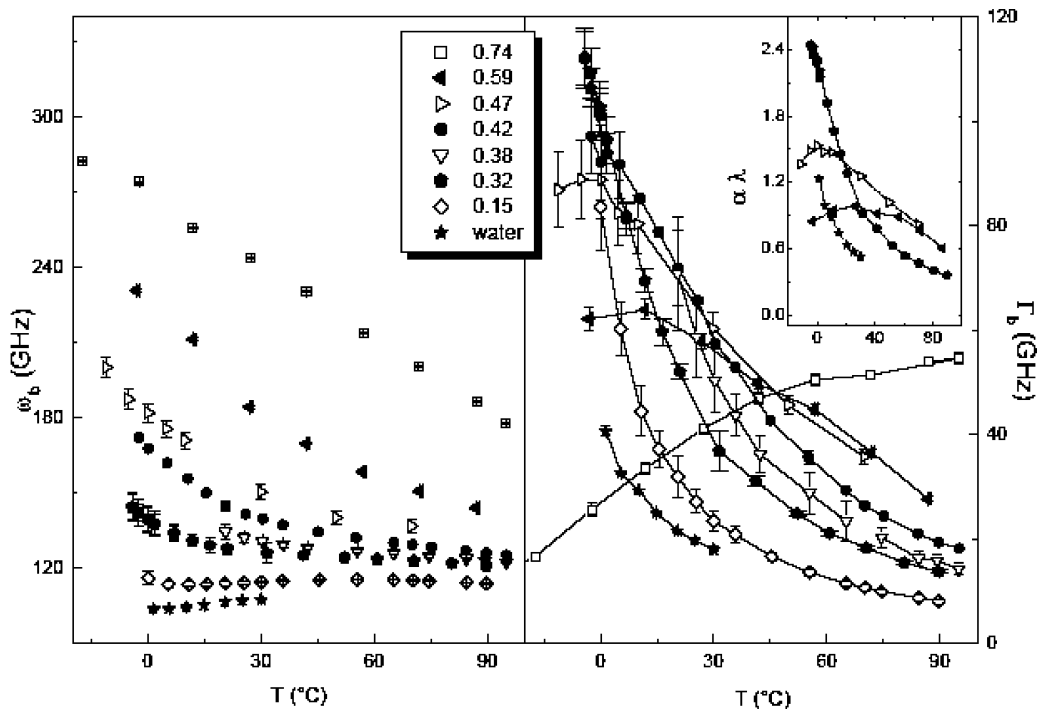


Figure 4. T dependence of ω_b and Γ_b for some selected ϕ values. Solid lines in the right panel are guides for the eye. Inset: $\alpha\lambda$ values for some representative concentrations.

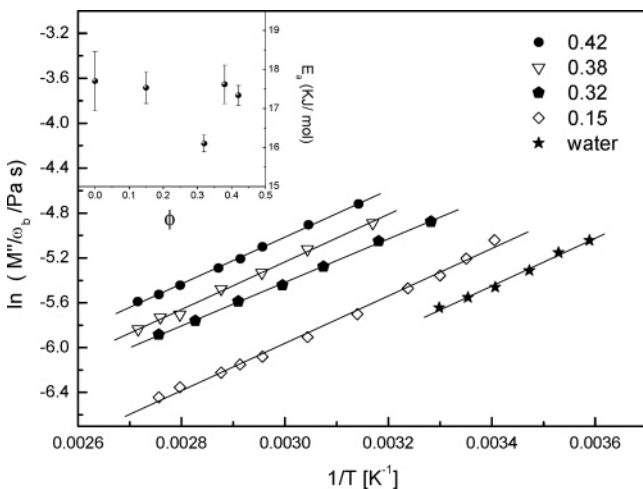


Figure 5. Values of M'' as a function of $1/T$ for pure water and low- ϕ solutions. The solid lines through the experimental data are linear fits. The corresponding activation energies are reported in the inset. This analysis was restricted to high- T , low- ϕ samples (see text).

respectively.^{27,29–31} On the other hand, it has been recently shown that, as a first approximation, an explicit T dependence of Δ can be neglected in the case of pure liquid water,³⁰ as well as in other liquid systems.³¹ By using eqs 3 and 4 and neglecting the T dependence of Δ , it is then possible to retrieve the value of E_a directly from the T dependencies of ω_b and Γ_b . Figure 5 shows the results of this analysis. It can be seen that experimental values of $\ln(M''(\omega_b)/\rho\omega_b)$ versus $1/T$ follow the expected linear dependence. Moreover, the calculated activation energies in the inset of Figure 5 are in agreement with the value of $E_a \approx 16 \pm 3$ kJ/mol, experimentally found for pure water.²⁹ It is worth mentioning that since eq 3 is valid for $\omega_b\tau \ll 1$, in Figure 5, only experimental data corresponding to dilute solutions at high T were considered.

For low T high ϕ solutions, a different strategy has been used in order to derive E_a . According to the memory function

framework,^{13,32} as a first approximation, the quantities $M'(\omega_b)Q^2/\rho$ and $M''(\omega_b)Q^2/(\rho\omega_b)$ can be written as:

$$M'(\omega_b)Q^2/\rho = (c_s Q)^2 + \Delta\xi^2/(1+\xi^2) \quad \text{and} \\ M''(\omega_b)Q^2/(\rho\omega_b) = \Delta\tau/(1+\xi^2) \quad (5)$$

where c_s is the adiabatic sound velocity and ξ is the dimensionless quantity $\omega_b\tau$. In order to derive eq 5, the following assumption were made: (i) there is only an active relaxation process in the considered frequency window, (ii) this relaxation is described by an exponential time decay (Debye relaxation function), and (iii) the specific heat ratio, γ , is equal to 1, thus, leading to negligible contributions of thermal fluctuations. The first two assumptions are consistent with those used in previous experiments,^{28–31} while the latter is justified by thermodynamic data for pure water.³⁵ By equating eqs 2 and 5, the following expression for the relaxation time can be derived:

$$\tau = \frac{1}{\Gamma_b} \left(1 - \frac{c_s^2 Q^2}{\omega_b^2} \right) \quad (6)$$

Equation 6 is meaningful only if $\omega_b \neq c_s Q$, that is, for $\xi \neq 0$, where the departure from the adiabatic regime takes place. Owing to the accuracy ($<1\%$) of our experimental determination of ω_b , slight departures from the adiabatic regime can be measured, and therefore, low values of τ can be determined. For this reason, the range where eq 6 can be meaningfully employed extends at high-temperature (i.e., at low τ), thus partially overlapping the range where eq 4 can be safely used. As a matter of fact, in the T range where both equations were used in order to determine E_a , the results obtained by using the two different methods are fully consistent. However, despite the accuracy of our experimental data, eq 6 is not applicable to the pure water, since we found that $\omega_b \approx c_s Q$ in the probed T range. Nonetheless, data of τ for pure water are already available in literature.²⁹ These data were derived by the analysis of $S(Q,\omega)$ determined by inelastic X-ray scattering (IXS) experiments.

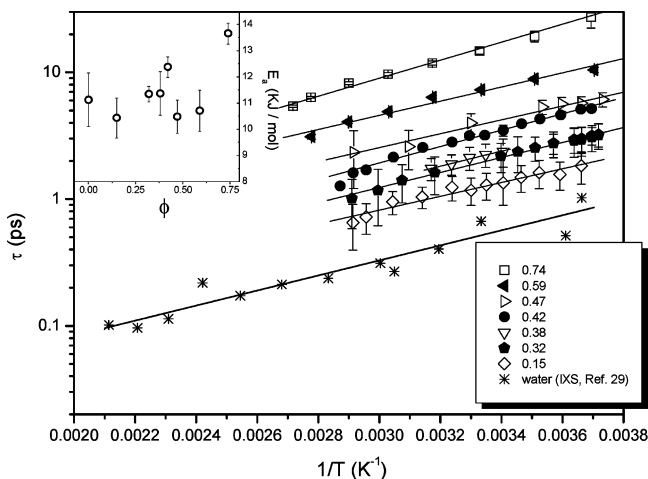


Figure 6. Structural relaxation time as a function of the inverse temperature. Data for pure water are taken from ref 29. In the inset the activation energy (E_a) is reported as a function of ϕ , as derived from the interpolation of the experimental data (see text for further details).

Owing to the wider (Q, ω) range accessed by IXS with respect to IUVS, a different data analysis strategy that does not rely upon approximate equations as eqs 4 and 6 has been employed.²⁹ The values of τ obtained by using eq 6 are reported in Figure 6 together with IXS data for pure water. This figure shows that by adding trehalose a progressive slowing-down of τ occurs at a given temperature. Furthermore, in the thermodynamic range spanned in the present experiment, the data can be described by an exponential (Arrhenius) T dependence, $\tau(T) = \tau_0 \exp(-E_a/k_B T)$, as previously supposed in deriving eq 4. The values of E_a are close to 12 kJ/mol up to the higher concentration levels. The slightly different values obtained by this procedure with respect to those estimated by means of eq 4 can be reasonably attributed to the different approximations involved in the two approaches.

However, in both cases, the values obtained for E_a are not appreciably dependent on the concentrations of the solutions and are in agreement with experimental determinations for pure water.²⁹ This result suggests that, at a given temperature, the whole dynamic mechanism remains substantially unperturbed in a quite large range of sugar concentration and is still governed by molecular H bonds.³⁷ However, while the energy of activation seemingly remains constant, an inverse correlation between temperature and concentration is evident in the structural relaxation times.

Quite similar conclusions have been reached in a number of recent investigations, mostly using neutron scattering experiments and MD simulations. By working with trehalose or glucose at concentrations of up to 50% (5 m), the claim has been made that the first hydration shell, dominated by HB, is not significantly perturbed even at fairly high concentrations³⁸ (1:10, glucose:water) and that no perturbation is observed for the trehalose solutions in confined space.¹¹ Attention is also addressed on the long-range structure of “bulk water” which does not seem affected by the solute, even at fairly high concentrations. An extensive slowing down of the water molecules surrounding the sugar has also been detected by depolarized Rayleigh scattering experiments^{39,40} showing the changes of structural dynamics between bulk and hydrating water at low and moderately concentrated sugar solutions.

While these studies provide support to the “pseudo-ideal” behavior of sugar–water systems, they also call for a better rationalization of the properties of the sugar “family”, including trehalose, at higher concentrations. In particular, the question

does not concern the obvious structural and dynamical changes of water molecules when in the hydration layers but the remaining water molecules distributed between these “clusters”.⁴¹ As far as the dynamical results of the present study are concerned, only a small increase of E_a of about 2 kJ/mol was found at the highest concentration, although this point needs further experimental verification. However, given the inverse T, ϕ correlation, a dramatic change of properties at low moisture content has to be expected.

Experiments in this direction are under way, as well as other investigations focused on covering the higher concentrations, up to pure undercooled trehalose. In particular, provided that a robust theoretical formalism can be used in the whole compositional range, the present results demonstrate that IUVS can give consistent information on the dynamics of water–trehalose solutions.

Conclusion

The results of the present study concern the structural relaxation time, τ , of the water–trehalose system and its evolution with increasing concentration and decreasing temperature. The study shows that aqueous trehalose solutions exhibit a slowing of the HB rearrangements upon increasing sugar concentration (or decreasing temperature). At molecular level, the small changes in the activation threshold of the relaxation have to be straightforwardly related to the continuous rearrangement of hydrogen bonds in the solution. Therefore, the biological action of trehalose can be only partially explained by the formation of an extensive layer of structured water which would affect the tetrahedral network of water. When trehalose is present in biological or cellular material at high concentrations, a “dramatic” rearrangement decrease of the HB of residual water at lower temperatures without crystallization might help to prevent embedded biomaterial from damage such as denaturation. However, the question about whether this development of mechanical properties is sufficient for the full explication of the higher bioprotective functions of trehalose, in comparison with other sugars, up to more concentrate systems is still a matter of discussion.

By looking at the bioprotective action developed in the biosystems, it seems necessary to resort to a certain amount of additional experimental evidence that has now been accumulated, at low moisture, for a parallel formation of nanocrystals of dihydrate crystals during dehydration of trehalose and other sugars.^{6–8,42} Therefore, as the potentially plasticizing water is captured in the dihydrate crystalline cage, the remaining dry amorphous trehalose enters the glassy state, and the whole matrix becomes much firmer, even if an apparent amount of water is still present. The relevance of the above data, within the hypotheses made in the present work, relies on the observed changes in the dynamics of the trehalose–water solutions upon increasing trehalose concentration. Although a continuous variation is observed, due to its modest magnitude, it can hardly be responsible for the expected strengthening in natural conditions. However, at ambient temperature, trehalose–water solutions enter the glassy phase upon the removal of water molecules because of both evaporation and crystallization or just one in confined nanocrystals. It is straightforward to conclude that both processes produce the desired results, but the extent of the resulting firmness and the rate of evolution could be very different.

Although our data cover a wide concentration range, experiments still need to be extended up to anhydrous trehalose, as well as in a wider wavelength range. In the future, our laboratory

plans to enrich this type of information and to investigate the subtle differences in homologous disaccharides.

Acknowledgment. We gratefully acknowledge the Structural Biology Lab group (Elettra) for the hospitality and access to instrumentation, in particular, Ivet Krastanova and Theodora Zlateva, for their patient support during sample preparation. We would also like to thank Riccardo Comin for his valuable contribution during the experiments. O.D.G. is grateful to the University of Trieste for the financial support of the Ph.D. Fellowship.

References and Notes

- (1) Carpenter, J. F.; Crowe, J. H. *Biochemistry* **1989**, *28*, 3916.
- (2) Crowe, J. H.; Crowe, L. M. *Nat. Biotechnol.* **2000**, *18*, 145.
- (3) Villarreal, M. A.; Diaz, S. B.; Disalvo, E. A.; Montich, G. G. *Langmuir* **2004**, *20*, 7844.
- (4) Ding, S.-P.; Fan, J.; Green, J. L.; Lu, Q.; Sanchez, E.; Angell, C. A. *J. Thermal Anal.* **1996**, *47*, 1391.
- (5) Branca, C.; Magazù, S.; Maisano, G.; Migliardo, P. *J. Chem. Phys.* **1999**, *111*, 2081.
- (6) Cesàro, A. *Nat. Mater.* **2006**, *5*, 593.
- (7) Sussich, F.; Urbani, R.; Princivalle, F.; Cesàro, A. *J. Am. Chem. Soc.* **1998**, *31*, 7893.
- (8) Sussich, F.; Skopec, C.; Brady, J.; Cesàro, A. *Carbohydr. Res.* **2001**, *334*, 165.
- (9) Ekdawi-Sever, N. C.; Conrad, P. B.; de Pablo, J. J. *J. Phys. Chem. A* **2001**, *105*, 734.
- (10) Liu, Q.; Schmidt, R. K.; Teo, B.; Karplus, P. A.; Brady, J. W. *J. Am. Chem. Soc.* **1997**, *119*, 785.
- (11) Lelong, G.; Price, D. L.; Brady, J. W.; Saboungi, M.-L. *J. Chem. Phys.* **2007**, *127*, 065102 and references therein.
- (12) Slie, W. M.; Donfor, A. R.; Litovitz, T. A. *J. Chem. Phys.* **1966**, *44*, 3712.
- (13) Boon, J. P.; Yip, S. *Molecular Hydrodynamics*; Dover: New York, 1991.
- (14) Cesàro, A.; Gamini, A.; De Giacomo, O.; Masciovecchio, C.; Gessini, A.; Di Fonzo, S. *Philos. Mag.* **2006**, *87*, 623.
- (15) D(+)- Trehalose Dihydrate T 9449–100G from Sigma, U.S.A., Batch # 114K7064.
- (16) Mehl, P. M. *J. Therm. Anal.* **1997**, *49*, 817.
- (17) Miller, D. P.; de Pablo, J. J.; Corti, H. *Pharm. Res.* **1997**, *14*, 578.
- (18) Gordon, M.; Taylor, J. S. *J. Appl. Chem.* **1952**, *2*, 493. In the calculation of T_g , we assumed a value of $k = 5.2$ and 394.2 K and 138 K for the glass transition temperatures of pure trehalose and water, respectively.
- (19) Chen, T.; Fowler, A.; Toner, M. *Cryobiology* **2000**, *40*, 277.
- (20) Masciovecchio, C.; Cocco, D.; Gessini, A. *Proceedings of 8th International Conference of Synchrotron Radiation Instrumentation*; San Francisco, California, August 25–29, 2003.
- (21) Czerny, M.; Turner, A. F. Z. *Physik* **1930**, *61*, 792.
- (22) Zaidi, A. A.; Makdisi, Y.; Bhatia, K. S.; Abutahun, I. *Rev. Sci. Instrum.* **1989**, *60*, 803.
- (23) Berne, B. J.; Pecora, R. *Dynamic Light Scattering*; J. Wiley & Sons: New York, 1976.
- (24) Fak, B.; Dorner, B. *Institute Laue Langevin (Grenoble France) Tech. Rep. No. 92FA008S*, 1992.
- (25) More, J. J. *Numerical Analysis, Lecture Notes in Mathematics*; Watson, G. A., Ed.; Springer-Verlag: Berlin, 1997; Vol. 630, p 105.
- (26) Fioretto, D.; Comez, L.; Socino, G.; Verdini, L.; Corezzi, S.; Rolla, P. A. *Phys. Rev. E* **1999**, *99*, 1899.
- (27) Herzfeld, E.; Litovitz, T. A. *Absorption and Dispersion of Ultrasonic Waves*; Academic Press: New York, 1959.
- (28) Cunsolo A.; Nardone, M. *J. Chem. Phys.* **1996**, *105*, 3911.
- (29) Monaco, G.; Cunsolo, A.; Ruocco, G.; Sette, F. *Phys. Rev. E* **1999**, *60*, 5505.
- (30) Bencivenga, F.; Cunsolo, A.; Krisch, M.; Monaco, G.; Ruocco, G.; Sette, F. *Phys. Rev. E* **2007**, *75*, 051202.
- (31) Bencivenga, F.; Cunsolo, A.; Krisch, M.; Monaco, G.; Orsingher, L.; Ruocco, G.; Sette, F.; Vispa, A. *Phys. Rev. Lett.* **2007**, *98*, 085501.
- (32) Balucani, U.; Zoppi, M. *Dynamics of the Liquid State*; Clarendon Press: Oxford, 1994.
- (33) Torre, R.; Bartolini, P.; Righini, R. *Nature (London)* **2004**, *428*, 296.
- (34) Masciovecchio, C.; Santucci, S. C.; Gessini, A.; Di Fonzo, S.; Ruocco, G.; Sette, F. *Phys. Rev. Lett.* **2004**, *92*, 255507.
- (35) Release on the IAPWS Formulation 1995 for the Thermodynamic Properties of Ordinary Water Substance for General and Scientific Use, Fredericia, Denmark, September, 1996.
- (36) Magazù, S.; Migliardo, P. J.; Musolino, A. M.; Sciortino, M. T. *J. Phys. Chem. B* **1997**, *101*, 2348.
- (37) Eisenberg, D.; Kauzmann, W. *The Structure and Properties of Water*; Oxford Press: London, 1979; Chapter 4.6.
- (38) Mason, P. E.; Neilson, G. W.; Enderby, J. E.; Saboungi, M.-L.; Brady, J. W. *J. Phys. Chem. B* **2005**, *109*, 13104.
- (39) Fioretto, D.; Comez, L.; Gallina, M. E.; Morresi, A.; Palmieri, L.; Paolantoni, M.; Sassi, P.; Scarponi, F. *Chem. Phys. Lett.* **2007**, *441*, 232.
- (40) Paolantoni, M.; Sassi, P.; Morresi, A.; Santini, S. *J. Chem. Phys.* **2007**, *127*, 024504.
- (41) Lerbret, A.; Bordat, P.; Affouard, F.; Descamps, M.; Migliardo, F. *J. Phys. Chem. B* **2005**, *109*, 11046.
- (42) Sussich, F. Ph.D. Thesis, University of Trieste, 2004.